tga1 should not exist (9). The discovery of *tga1* also represents a case in which the evolution of a new adaptation was largely governed by a single locus, providing further evidence for the controversial view that evolution can proceed by a relatively few large steps (13). Because the development of Native American societies and the evolution of maize were intimately connected (14), the selection of *Tga1* by early maize agriculturists represents a critical event in the cultural history of the New World.

REFERENCES AND NOTES

1. G. W. Beadle, *Field Mus. Nat. Hist. Bull.* **43**, 2 (1972).
2. W. C. Galinat, *Annu. Rev. Genet.* **5**, 447 (1971).
3. J. F. Doebley, M. M. Goodman, C. W. Stuber, *Syst. Bot.* **9**, 203 (1984).
4. H. H. Iltis and J. F. Doebley, *Am. J. Bot.* **67**, 994 (1980).
5. T. A. Kato, *Res. Bull. Mass. Agric. Exp. St.* **635**, 1 (1976).
6. B. McClintock, T. A. Kato, A. Blumenschein, *Chromosome Constitution of Races of Maize* (Colegio de Postgraduados, Chapingo, Mexico, 1981).
7. G. W. Beadle, *J. Hered.* **30**, 245 (1939); *Sci. Am.* **242**, 112 (January 1980).
8. W. C. Galinat, *Maydica* **30**, 137 (1985).
9. H. H. Iltis, *Science* **222**, 886 (1983).
10. J. F. Doebley, A. Stec, J. F. Wendel, M. Edwards, *Proc. Natl. Acad. Sci. U.S.A.* **87**, 9888 (1990); J. F. Doebley and A. Stec, *Genetics* **129**, 285 (1991); ———, *ibid.* **134**, 559 (1993).
11. P. C. Mangelsdorf, *Adv. Genet.* **1**, 161 (1947); J. S. Rogers, *Genetics* **35**, 541 (1950); W. C. Galinat, *Econ. Bot.* **17**, 51 (1963).
12. Of the 212 progeny, there were 142 nonindurate and 70 indurate types. These numbers deviate from the expected 3:1 segregation ratio for a locus with dominant gene action. The RFLP loci deviated in the same fashion; for example, *UMC191* had a 27:113:90 ratio of maize homozygotes:heterozygotes:teosinte homozygotes, which deviates from the expected 1:2:1 segregation ratio for a codominant locus. These deviations reflect the different allelic constitutions of W22 and W22-TGA for a gametophytic incompatibility locus (CP2) located near *tga1* [J. L. Kermicle and J. O. Allen, *Maydica* **35**, 399 (1990)]. Although *tga1* behaves like a qualitative locus in the uniform genetic background of W22, its phenotypic expression can be affected by unlinked loci, causing it to behave more like a QTL in a heterogeneous genetic background [J. F. Doebley, J. E. Dorweiler, J. L. Kermicle, *Maize Genet. Coop. Newsl.* **66**, 95 (1992)].
13. H. A. Orr and J. A. Coyne, *Am. Nat.* **140**, 725 (1992).
14. K. V. Flannery, *Annu. Rev. Anthropol.* **2**, 271 (1973); C. B. Heiser, *Seed to Civilization: The Story of Food* (Freeman, San Francisco, CA, 1981), pp. 100–101.

15. We thank B. Burr, K. Cone, J. Gardiner, D. Grant, C. Hannah, and J. Rosichan for providing RFLP probes. Supported by National Science Foundation grant BSR9107175 and by the Charles J. Brand Fellowship (J.D.).

8 April 1993; accepted 18 August 1993

Mammalian Locomotor-Respiratory Integration: Implications for Diaphragmatic and Pulmonary Design

Dennis M. Bramble* and Farish A. Jenkins Jr.

Diaphragmatic function and intrapulmonary respiratory flow in running mammals were found to differ substantially from the corresponding conditions known in resting mammals. In trotting dogs, orbital oscillations of the diaphragm were driven by inertial displacements of the viscera induced by locomotion. In turn, oscillations of the visceral mass drove pulmonary ventilation independent of diaphragmatic contractions, which primarily served to modulate visceral kinetics. Visceral displacements and loading of the anterior chest wall by the forelimbs are among the factors that contribute to an asynchronous ventilation of the lungs and interlobar gas recycling. Basic features of mammalian respiratory design, including the structure of the diaphragm and lobation of the lungs, appear to reflect the mechanical requirements of locomotor-respiratory integration.

Mammals, among the most active of vertebrates, have evolved respiratory and locomotor systems of complex and distinctive design. Despite substantial interest focused on the mechanical basis of mammalian respiration, numerous aspects of the respiratory system, including diaphragmatic structure, pulmonary lobation, and right-left asymmetry of the lungs, are as yet poorly understood. In reality the thoracic complex of mammals is inextricably linked to both respiration and locomotion, and the demands of both are intensified during exercise (1). Reptiles, in contrast, appear unable to achieve effective lung ventilation during rapid locomotion; a mechanical constraint on simultaneous running and breathing is probably primitive for tetrapods (2). The ability to integrate locomotor and respiratory mechanics appears to be an evolutionarily derived feature that has been critical to developing the elevated aerobic capacity and stamina that distinguishes mammals and birds (2, 3).

In stationary mammals, contraction of the diaphragm provides a primary mechanical drive for inspiration. In running mammals, inertial oscillations of the abdominal viscera and the movements of the trunk have been hypothesized as influencing diaphragmatic mechanics in a manner that tends to synchronize respiration with locomotion (4). Observations of coupling ratios between breathing and gait cycles in various mammals have been cited in support of such a mechanical integration (1, 5), but the significance of this phenomenon has remained controversial (6) in the absence of direct observations of diaphragmatic or visceral motion in active animals. We present a cineradiographic analysis of diaphragmatic, trunk, and chest wall movements in trotting dogs (7) and infer previously unknown patterns of gas flow within the lungs that result from locomotor-respiratory interactions.

In trotting, contralateral pairs of fore- and hindlimbs alternate in providing support and propulsion. Cyclical variations in vertical and horizontal accelerations of the body occur in conjunction with the contact phase of each limb pair. During the initial part of the contact phase (Fig. 1, phases A and B), the trunk sinks downward, decelerating horizontally and vertically (Fig. 1, G through I); during the second half of the contact phase, the body accelerates upward and forward (Fig. 1, G through I; phases B and C). Although the acceleration-deceleration profiles are consistent for all dogs, the vertical oscillations, which occur twice in each stride cycle, are not invariably symmetric; greater vertical excursion commonly occurs during the contact phase of a particular forelimb (usually the right) (Fig. 1G). The displacements of the diaphragm appear to result primarily from the inertial oscillations of the pendulous visceral mass within the abdomen and in particular the liver, which is attached centrally to the diaphragm. When the trunk decelerates during the initial part of a contact phase, the viscera displace the diaphragm craniad (Fig. 1J; phases A and B). Conversely, when the trunk subsequently accelerates forward and upward, the diaphragm follows the visceral mass caudad (Fig. 1J; phases B and C). As expected, the primary respiratory cycle of inspiration and expiration closely tracks the movements of the oscillating diaphragm (Fig. 1K) (8).

Excursions of the viscera during trotting are affected not only by the kinetic oscillations of the trunk but also by the physiological state of the diaphragm, which we infer from cineradiographic observations. Excursions of the inactive diaphragm are larger than those during contractions

D. M. Bramble, Department of Biology, University of Utah, Salt Lake City, UT 84112.
F. A. Jenkins Jr., Department of Organismic and Evolutionary Biology, and Museum of Comparative Zoology, Harvard University, Cambridge, MA 02138.

*To whom correspondence should be addressed.

(hatching, Fig. 2A) when the diaphragm restrains the anterior displacement of the viscera. A diaphragmatic contraction is thus identified by a characteristic kinematic profile: positions recorded in successive cineradiographic frames are closely juxtaposed (Fig. 2B) as a result of the increased stiffness of the membrane, in contrast to the greater displacements observed when the diaphragm is relaxed and more compliant. A contraction is also evident on the basis of a change in the outline of the diaphragm seen in lateral projection. The dorsal region of the diaphragm, representing the crural part, is more or less straight or slightly concave when relaxed (Fig. 3, A and B) but bulges to a convex outline when contracted (Fig. 3, C and D).

Pneumotachographic recordings obtained simultaneously with cineradiographs of diaphragmatic movements show no simple 1:1 relation between respiratory frequency and diaphragmatic contractions. Breathing rates always exceed diaphragmatic contraction rates, the ratio varying from 3:1 to nearly 10:1 (9). Contractions of the diaphragm occur in various ratios to the stride cycle: 1:1 (Fig. 2A), 1:4 (Fig. 2C), and other combinations (*10*). Diaphragmatic contractions interrupt the phasic relation between the inertial oscillations of the diaphragm and the respiratory cycle that develops when the diaphragm undergoes several consecutive oscillations in a relaxed state (that is, in instances of a 4:1 ratio between stride cycle and diaphragmatic contraction; Fig. 2C). After a diaphragmatic contraction, respiratory flow initially lags diaphragmatic displacement (Fig. 2D); the phase lag progressively declines to zero, at which point another contraction intervenes to reset the diaphragm to continue free oscillation of the visceral mass from a more caudal position (*11*).

An unexpected finding is that cycles of expiratory and inspiratory flow continue uninterrupted during diaphragmatic contractions; expiration during diaphragmatic contraction and posterior movement of the viscera is paradoxical (Fig. 2). An explanation of this phenomenon derives from the fact that diaphragmatic-visceral movements, rather than the simple linear displacements assumed by visceral piston models (*12*), are complex. The alternating deceleration and acceleration of the trunk in the horizontal and vertical planes imparts an elliptical orbit to the visceral mass (*13*). Thus, the diaphragm has not only an anteroposterior excursion (Fig. 3, *x*) but also a dorsoventral excursion (Fig. 3, *y*). The relative proportions of the *x* and *y* displacements are in turn modulated by the contractile state of the diaphragm. When the diaphragm is relaxed and compliant, anteroposterior and dorsoventral displacements are approximately equal (Fig. 3, A and B). During a contraction, the stiffened diaphragm retracts against the viscera and thus damps the anteroposterior component of the inertial oscillations (Fig. 3, bottom; *x*, hatching). However, neither the costal nor the crural parts of the diaphragm, both of which have more or less longitudinally oriented fibers, can effectively restrain dorsoventral displacements of the viscera, which therefore continue to drive ventilation throughout a contraction (Fig. 3, C and D). These dorsoventral excursions principally impact the caudal part of the diaphragmatic lobes of the lungs, which in dogs and many other mammals extend above the viscera.

In addition to the inertial oscillations of the viscera and the variable compliance of the diaphragm, another mechanical factor,

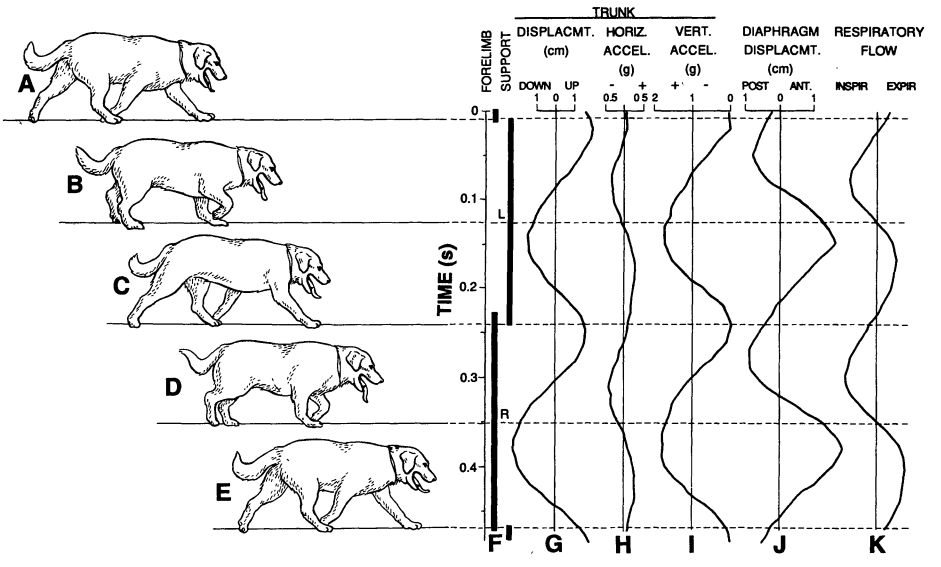

Fig. 1. The stride cycle in a trotting dog (**A** through **F**) with kinematic data on the trunk (**G** through **I**) and diaphragm (**J**), and a pneumotachographic record of inspiration and expiration (**K**), all synchronously recorded (*7*).

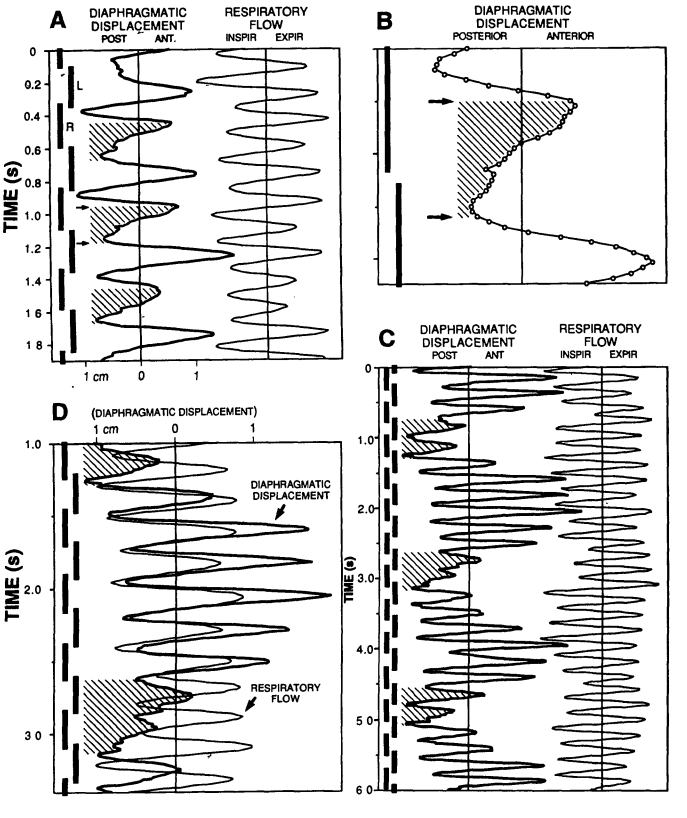

Fig. 2. Phasic relations of respiratory flow and the anteroposterior displacements of the diaphragm in trotting dogs. Right and left forelimb support is indicated by bars (R, L). Diaphragmatic contractions are shown by hatching. The contraction episode indicated with arrows in (**A**) is enlarged in (**B**) to reveal the diminished velocity (closely spaced data points) that is characteristic of the activated, stiffened diaphragm. Diaphragmatic displacements and respiratory flow in (**C**) are superimposed in (**D**) to illustrate phase shifting that characterizes periods of diaphragmatic relaxation.

chest wall loading, directly impacts the lungs. The two sides of the thorax are alternately deformed during trotting by the transfer of weight to the load-bearing forelimb. Cineradiographic films taken in ventrodorsal projection reveal that the first five ribs of the loaded chest wall are deflected posteromedially in series from front to back as the chest moves forward over the supporting limb (Fig. 4, left). This deformation, which begins during the first half of the contact phase of each forelimb and is mediated by slips of the serratus ventralis muscle, compresses the adjacent part of the lung (the apical, or cranial, lobe). On the contralateral, non–weight-bearing side, the ribs shift anterolaterally as the limb is being protracted, expanding this part of the chest wall to its unloaded, convex form (Fig. 4, right).

The dimensions of the lungs, intimately fitted to the walls of the chest, are therefore mechanically modified during trotting by locomotor-induced forces. Evidence that these forces produce differential volumetric changes within the lungs is provided by the cineradiographic films themselves. Utilizing a rear-projection film analyzer, we apposed photocells to the displayed lobar fields (apical, cardiac, and diaphragmatic) in lateral-projection cineradiographs and recorded the variations in radiodensity, which are directly related to fluctuations in the amount of respired air present in a particular lobe (*14*). Despite differences in trotting speed and respiratory rate between individual records, the filling and emptying of the apical and diaphragmatic lobes were invariably found to be out of phase (Fig. 5, A and B). Furthermore, the radiodensity-volume (RDV) curves, which represent the composite density of paired (right and left) lobes, are themselves asymmetrical. In the case of apical lobes, for example, major peaks alternate with minor peaks. This asymmetry is explicable in terms of the fact that the right apical lobe is larger than the left; the lobe contralateral to the supporting limb is preferentially filled because the lobe on the side of the supporting limb is being subjected to thoracic compression (Fig. 4). Thus, we would interpret the major peaks (which occur at the end of the left forelimb's support phase) as primarily representing filling episodes of the right apical lobe, and minor peaks as filling episodes of the left apical lobe (*15*).

On the basis of synchronized records of diaphragmatic excursions, respiratory and locomotor cycles, and RDV curves derived from cineradiographic films, we propose a model of pulmonary ventilation in trotting dogs that accounts for the complex interaction of forces and flow (Fig. 6) (*16*). We suggest that ventilation of the diaphragmatic lobes is principally a function of the kinetics of the neighboring visceral mass, whereas ventilation of the apical lobes is dictated by the loading pattern of the adjacent chest walls. During inspiration, which typically occurs early in the support phase of a forelimb, air is drawn into the diaphragmatic lobes by the posteroventral displacement of the viscera; simultaneously, the chest wall on the side of the supporting forelimb is compressed, expelling air from the adjacent apical lobe into the airstream directed into the ipsilateral diaphragmatic lobe (Fig. 6, A and C). During expiration, air is expelled from the diaphragmatic lobes by the anterodorsal displacement of the viscera. Air from the diaphragmatic lobe contralateral to the side of the supporting forelimb flows into the trachea and is also induced into the ipsilateral apical lobe by the expansion of the adjacent chest wall that accompanies protraction of the swing phase limb (Fig. 6, B and D). The diverted airstream would comprise at least in part the unrespired tidal volume that reached the bronchi but not the alveoli. A similar diversion of the flow from the diaphragmatic to apical lobe on the supporting limb side is precluded by the compressive loading of the chest wall. The anteriorly directed secondary bronchi of the apical lobes, represented in Fig. 6 on the basis of anatomical preparations (*17*), are suitably arranged to capture part of the airstream expelled from the ipsilateral diaphragmatic lobe during expiration as well as to direct expelled air into the same lobe during inspiration.

The subdivision of the lungs into discrete mechanical units, or lobes, permits some regions to be filled while others are emptied. The three major lobes common to most mammals (apical, cardiac, and diaphragmatic) correspond to the three separate sources of loading for the pleural surfaces (anterior chest wall, heart, and diaphragm plus viscera). Interlobar fissures thus appear to represent shear zones that, if the lung tissue were continuous, would be stressed by adjacent forces of distension and compression. We hypothesize, on the basis of the widespread occurrence of lobation in mammals, that locomotor-respiratory interactions similar to those in dogs developed early in mammalian history. The common pattern of three lobes in the left lung and

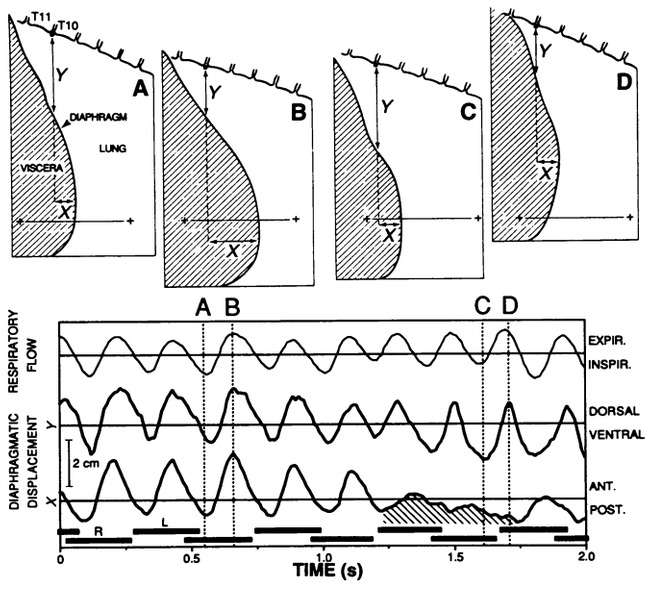

Fig. 3. (**Top**) Diaphragmatic profiles traced from a lateral-projection cineradiographic film of a trotting dog. A pair of registration marks on the image intensifier are denoted by + +; the line between them represents a fixed gravitational horizontal. Note the vertical displacements of the trunk. Anteroposterior (*x*) and dorsoventral (*y*) excursions of the diaphragm were measured relative to the ventral margin of the intervertebral disk between the 10th and 11th thoracic vertebrae (T10, T11). The range of positions of the diaphragm is shown in a freely oscillating (inactive) state (**A** and **B**) and during a contraction (**C** and **D**). (**Bottom**) Respiratory flow synchronously recorded with *x* and *y* displacements of the diaphragm. The position of the cineradiographic frames depicted in panels (A through D) above are located in this sequence. As in Fig. 2, right and left forelimb support is indicated by bars (R, L), and the duration of a diaphragmatic contraction is shown by hatching.

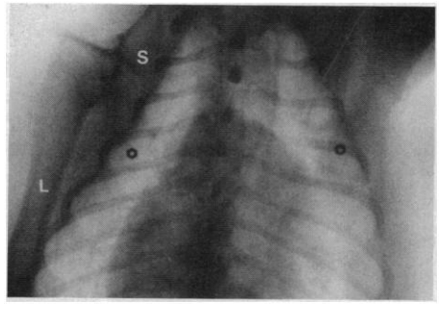

Fig. 4. Cineradiographic image taken in ventrodorsal projection of the chest in a trotting dog. The left (L) forelimb is load-bearing (in a position comparable to that shown in Fig. 1C). Note the scapula (S), the compression of the adjacent thoracic wall, and the relatively large size of the right apical lobe.

four in the right is known in representatives of diverse mammalian orders, including Artiodactyla, Lagomorpha, Rodentia, Carnivora, and nonhuman primates (*18*). However, in other groups the number and degree of differentiation of lobes vary. In small rodents and in some bats, lobation is present only on the right side. Additionally, a right-left asymmetry in lung size is characteristic of most terrestrial mammals; the right lung is significantly larger than the left and incorporates an accessory lobe not present on the left side. Attempts to account for right-sided dominance on the basis of cardiac positioning (for example, as in humans) are insufficient given the midline or dextral position of the heart in many mammals. A more plausible explanation, in terms of locomotor-respiratory interactions, is that the dextrally placed liver favors a biased investment in the right lung in terms of size and lobation; the liver is the largest and most consistent of the abdominal organs in mass and shape and therefore is mechanically the most reliable driver. A related bias is present in the crural diaphragm where typically the right crus is more robustly developed than the left.

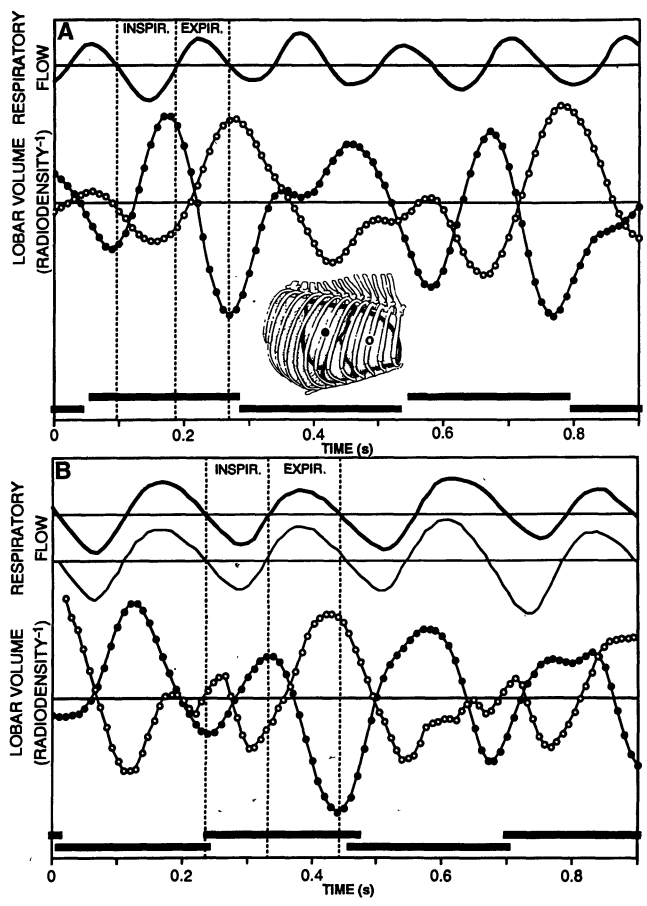

Fig. 5. Respiratory flow and changes in lobar volume recorded from local variations in radiodensity within the pulmonary field of a trotting dog. Because radiodensity decreases with lung inflation, the relative filling and emptying curves of the apical (○) and diaphragmatic (●) lobes are represented in terms of radiodensity^{-1}. (**A**) Simultaneously recorded apical and diaphragmatic lobar volumes and the associated respiratory flow. (**B**) Serially acquired records from the same trotting sequence superimposed with reference to respiratory flow (*28*). Upper (dark) line shows the respiratory flow recorded with radiodensity changes in the diaphragmatic lobe; lower (light) line is the apical lobe.

Further insight into the gross design of the lung may be derived from species in which lobation is vestigial or absent altogether. In horses, only the accessory lobe of the right lung is distinct; although cranial and caudal lobes are recognized on the basis of bronchial distribution, the rigidity of the equine thorax would appear to preclude significant thoracic deformation (*19*). The complete lack of lobation in marine mammals [dugongs, seals, and whales (*20*)] appears to be secondary and associated with other fundamental alterations of their locomotor and respiratory systems: the chest walls no longer receive sustained impulsive loading from the limbs, and respiration is discontinuous.

The diaphragm is recognized as a compound structure on the basis of its costal and crural divisions as well as innervation and development (*21*), but the functional significance of this duality has been unclear. We suggest that the crural diaphragm is a variable-length tether that primarily modulates the inertial oscillations of the viscera, which, during rapid locomotion, provide a major component of respiratory drive. The crura are mechanically suited to this purpose because they originate from a stable base (the lumbar vertebrae), in contrast to the fibers of the costal diaphragm which originate from mobile ribs. This interpretation is supported by the develop-

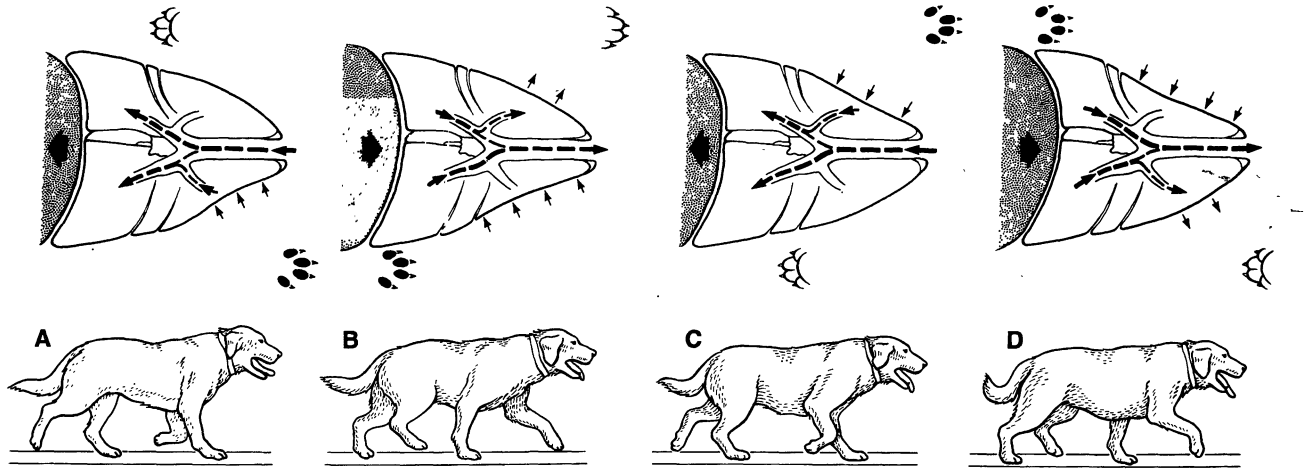

Fig. 6. A model of locomotor-respiratory dynamics in a trotting dog relating the influence of diaphragmatic oscillations (large arrows) and chest wall deformation (small arrows) to pulmonary flow. (**Top**) The lungs and visceral mass are represented in dorsal view; the positions of the supporting forefoot are indicated by black footprints. (**Bottom**) The corresponding phases of the gait cycle (**A** through **D**); (D) is comparable to the cineradiograph shown in Fig. 4.

ment of the crura, which arise from a muscularization of the dorsal, suspensory mesentery of the foregut (*22*). The costal diaphragm may participate in locomotor-induced ventilatory mechanics through the "diaphragmatic ligament," a thin, but elastin-rich sheet applied to the entire pleural surface of the muscular diaphragm; by passively absorbing the kinetic energy of the visceral mass, the diaphragmatic ligament may both safeguard against hyperextension of muscle fibers and provide elastic recoil that assists inspiration (*23*) even when the diaphragm is relaxed. The diaphragm thus incorporates major features that are integral to the mechanical effects and respiratory demands of locomotion.

Although regional heterogeneities in gas distribution within the mammalian lung are well documented (*24*), existing models do not anticipate the asynchronous interlobar exchange observed in trotting dogs. Models of differential flow at airway bifurcations invoke the balance of downstream loads to account for gas distribution (*25*) or emphasize fluid dynamic forces attributable to the geometry of the central airways, particularly the branching angles of daughter from parent ducts (*26*). The convective momentum of air moving down a primary bronchus will favor its continuation at a branch point along that pathway (secondary bronchus) having the smaller branching angle (for example, branches of the diaphragmatic rather than apical lobes, Fig. 6, A and C).

Among the potential physiological benefits of the relatively high-frequency interlobar exchange depicted in our model may be a more thorough mixing of airway gases and thereby a lesser likelihood of longitudinal airway stratification, which could reduce gas exchange efficiency (*27*). Moreover, asynchronous lobar ventilation may help to minimize a basic limitation of the tetrapod breathing apparatus: the wasted (dead space) ventilation intrinsic to tidal airflow.

REFERENCES AND NOTES

1. D. M. Bramble, *Am. Zool.* **29**, 171 (1989).
2. D. R. Carrier, *Exp. Biol.* **47**, 33 (1987); *Paleobiology* **13**, 326 (1987).
3. D. M. Bramble and F. A. Jenkins Jr., in *Complex Organismal Functions: Integration and Evolution In Vertebrates*, D. B. Wake and G. Roth, Eds. (Wiley-Interscience, Chicester, UK, 1989), pp. 133–146.
4. D. M. Bramble and D. R. Carrier, *Science* **219**, 251 (1983).
5. D. P. Attenburrow, *Equine Vet. J.* **14**, 69 (1982); R. V. Baudinette, B. J. Gannon, W. B. Runciman, S. Wells, J. B. Love, *J. Exp Biol.* **129**, 251 (1987); I. S. Young, R. D. Warren, J. D. Altringham, *ibid.* **164**, 283 (1992).
6. R. B. Banzett, J. Mead, M. B. Reid, G. P. Topulos, *J. Appl. Physiol.* **72**, 1922 (1992).
7. Four dogs (one male beagle, 15 kg; one male golden retriever, 30 kg; two female yellow labradors, average weight 24 kg) were trained to trot on a treadmill operated at 6 to 8.5 km/hour. All animal handling and care were in accordance with institutional guidelines. Siemens cineradiographic apparatus, positioned for either lateral or ventrodorsal projection, provided radiographic imaging of the chest and shoulder, which was recorded by a high-speed 16-mm cine camera mounted on the image intensifier and operated at 100 frames per second. Cineradiographic films documenting over 300 stride cycles were analyzed frame by frame on a Vanguard film analyzer with *x-y* coordinate verniers. We determined trunk displacements by tracking the ventral margin of an intervertebral space (usually T10–T11) relative to radiopaque markers set 10 cm apart and fixed to the image intensifier; displacement of the liver and diaphragm within the thorax were measured with reference to the same intervertebral point (see Fig. 3). Absolute scaling of all kinematic variables was by reference to a 2-cm radiopaque scale set on the midline of the dog's back.
8. Inspiratory-expiratory phases were recorded from two dogs (yellow labradors) with a mask-mounted pneumotach and stored on a TEAC CT-90 II tape recorder together with synchronization signals from the cineradiographic camera as well as a second camera (100 frames per second) recording the footfall sequence on conventional (light) film. Treadmill speed for pneumotach experiments was 8.5 km/hour; over 150 stride cycles were analyzed. Both subjects utilized relatively high-frequency (4.5 to 6.2 Hz), pant-like breathing, even when running in cool air (20° to 22°C). Exercising dogs readily shift to panting in order to dissipate metabolic heat [M. B. Goldberg, V. A. Langman, C. R. Taylor, *Resp. Physiol.* **43**, 327 (1981)]. A low-volume (8 cm^3), low-impedance screen pneumotach was connected to a Grass PT5A differential pressure transducer by means of pairs of polyethylene tubing (73 cm long, 1.5 mm inside diameter, 2 mm outside diameter). The frequency response was adequate (phase lag <1.5% up to 30 Hz). Cross-correlation analysis revealed a regular time delay of 25 to 35 ms between kinematic events at the diaphragmatic-pleural interface and flow response at the mouth, thus defining the time constant of the respiratory system. To better visualize kinematic-flow relationships, the pneumotach tracings in all figures have been time-shifted (leftward) 3 frames (=30 ms) to eliminate this time delay. To minimize impedance to respiratory flow, the face masks were not sealed; therefore, we have not quantified flow and volume.
9. Using electromyography, D. M. Ainsworth, C. A. Smith, S. W. Eicker, K. S. Henderson, and J. A. Dempsey [*Resp. Physiol.* **78**, 145 (1989)] demonstrated a 1:1 relation between diaphragmatic contraction and inspiratory airflow in slowly trotting dogs. However, their animals were constrained by face mask impedance to abnormally low breathing rates (<0.8 Hz).
10. Substitution of inertially powered oscillations of the diaphragm for contractions may contribute to the stamina that dogs display in trotting. Several conditions are known to produce diaphragmatic fatigue in mammals, including prolonged activity under high work loads [C. Roussos and P. T. Macklem, in *Handbook of Physiology: The Respiratory System* (American Physiological Society, Bethesda, MD, 1986), vol. 3, chap. 29]. The canine diaphragm is composed of fatigue-resistant fibers [D. F. Rochester, *J. Clin. Invest.* **75**, 1397 (1985)].
11. The phase relations between diaphragmatic motion and respiratory flow in trotting dogs differ from those of slowly breathing mammals. In all dogs (running or standing) with breathing frequencies greater than 1.5 Hz, flow was in phase with the acceleration of the diaphragm (plus visceral mass) and out of phase with velocity. Peak flows occur at (or near) the ends of the diaphragmatic excursion cycle. Undamped oscillations of the visceral piston appear to impart a driving force (inspiratory or expiratory) to the lungs that is proportional to displacement (on both *x* and *y* axes) from a central "resting position" that is neutral with respect to force production. The mean resting position corresponds to the statistical midpoint of the swing cycles of the diaphragm and viscera (that is, the zero line, Fig. 2D).
12. D. M. Bramble, in *Nonlinear Oscillations in Biology and Chemistry*, H. G. Othmer, Ed. (Springer-Verlag, Berlin, 1986), pp. 130–149; R. McN. Alexander, *J. Zool. (London)* **218**, 69 (1989); I. S. Young, R. McN. Alexander, A. J. Woakes, P. J. Butler, L. Anderson, *J. Exp. Biol.* **166**, 19 (1992).
13. In trotting dogs the transversus abdominis muscle may be activated during the contact phase of each limb pair (*9*). It is probable that the phasic contraction of the abdominal muscles both supports the viscera from below and contributes to their dorsal displacement.
14. Changes in current through photo cells (Radio Shack 276-196) were passed through a current-to-voltage converter. The signals were processed by a low-pass, six-order, slight dips active filter [D. Lancaster, *Active Filter Cookbook* (H. W. Sams, Carmel, IN, 1975)] with a cutoff frequency of 20 Hz and a rolloff slope of −36 dB per octave. The filtered signal was digitized by an 8-bit analog-to-digital converter at a sampling rate of 500 Hz (bandwidth, 250 Hz), and stored and analyzed with a Macintosh SE/30 computer. Verification that radiodensity data reflected changes in local lung volume was undertaken by three tests. (i) In awake, standing dogs, radiodensity data consistently matched inspiration and expiration in phase, polarity, and relative amplitude. (ii) Similar results were obtained from artificially ventilated, anesthetized dogs in a supine position. Dogs were induced and maintained on a surgical plane of anesthesia with 2% solution of thiamylal sodium (Bio-tel, Bio-Ceutic Division, Boehringer Ingelheim Animal Health, Inc.), intubated and placed on a ventilator (Harvard Apparatus model 708). (iii) Radiodensity data were found to be significantly correlated (mean r^2 = 0.958) with changes in lung volume in two euthanized rabbits (average weight 3.7 kg) in which the lungs were step-inflated at 10-cm^3 increments with a syringe. The trachea was exposed, transected, and intubated, and the intubation point was sealed with ethyl-2-cyanoacrylate. Similar pulmonary densitometry studies of resting and anesthetized mammals were undertaken by J. W. Laws and R. E. Steiner [*Br. J. Radiol.* **38**, 512 (1965)] and N. R. Silverman, M. Intaglietta, and W. R. Tompkins [*J. Appl. Physiol.* **34**, 726 (1973)].
15. Irregularities in the left apical RDV curves are due to the shadowing effect of the right limb, which was magnified by being farthest from the image intensifier. To evaluate the potential bias of a locomotor artifact, we examined RDV data from standing, panting dogs. These data were of uniform amplitude (indicating simultaneous filling-emptying of both apical lobes). Comparison of simultaneously acquired RDV data from apical and diaphragmatic lobes revealed both in-phase and out-of-phase patterns, as well as transitions between the two. Dogs therefore appear to be able to modulate the ventilatory phases of the apical and diaphragmatic lobes even while stationary. The RDV readings from the diaphragmatic lobes were selected in a manner that avoided possible contamination from neighboring structures (that is, ribs, diaphragm, viscera, great vessels).
16. This model applies specifically to episodes of sustained diaphragmatic relaxation and free oscillation of the visceral mass, as in Fig. 2, C and D. A more complex pattern of locomotor-respiratory interactions characterizes brief periods of diaphragmatic contraction as well as those situations in which the muscle is recruited more frequently (Fig. 2A).
17. Data on freshly excised dog lungs, inflated by constant pressure through the trachea and air-dried, confirm data on the configuration of the canine bronchial tree given by K. Horsfield, in *Gas Mixing and Distribution in the Lung*, L. A. Engel and M. Paiva, Eds. (Dekker, New York, 1985), pp. 23–61.
18. W. S. Tyler and M. D. Julian, in *Comparative*

Biology of the Normal Lung, R. A. Parent, Ed. (CRC Press, Boca Raton, FL, 1991), vol. 1, chap. 4.
19. D. E. Leith and J. R. Gillespie, *Fed. Proc. Fed. Am. Soc. Exp. Biol.* **30**, 556 (1971); A. M. Koterba, P. C. Kosch, J. Beech, T. Whitlock, *J. Appl. Physiol.* **64**, 337 (1988).
20. E. J. Slijper, *Whales* (Basic Books, New York, 1962), p. 140.
21. A. De Troyer, M. Sampson, S. Sigrist, P. T. Macklem, *Science* **213**, 237 (1981); A. De Troyer and S. H. Loring, in *Handbook of Physiology: The Respiratory System* (American Physiological Society, Bethesda, MD, 1986), vol. 3, chap. 26.
22. L. J. Wells, *Contrib. Embryol.* **35**, 107 (1954).
23. R. I. Griffiths, R. E. Shadwick, and P. J. Berger [*Proc. R. Soc. London Ser. B* **249**, 199 (1992)] described the "diaphragmatic ligament" in sheep but reported the presence of a similar structure in horses, cattle, rabbits, sea lions, and humans. We here confirm, on the basis of gross anatomical and histological observations, that dogs also have such a ligament.
24. J. B. West, *Regional Differences in the Lung* (Academic Press, New York, 1977); M. Paiva and L. A. Engel, in *Respiratory Physiology: An Analytical Approach*, H. K. Chang and M. Paiva, Eds. (Dekker, New York, 1989), pp. 245–276.
25. A. B. Otis *et al.*, *J. Appl. Physiol.* **8**, 427 (1956).
26. J. L. Allen, I. D. Frantz, J. J. Fredberg, *ibid.* **62**, 223 (1987); A. Tsuda and J. J. Fredberg, *ibid.* **69**, 546 (1990); A. Tsuda, R. Kamm, J. J. Fredberg, *ibid.*, p. 553.
27. J. Piiper and P. Scheid, in *Comparative Pulmonary Physiology: Current Concepts*, S. C. Wood, Ed. (Dekker, New York, 1989), pp. 369–416; E. R. Weibel, *The Pathway for Oxygen* (Harvard Univ. Press, Cambridge, 1984).
28. Radiodensity data were collected from the apical and diaphragmatic lobes separately (3.7 s apart) during the same trotting sequence when the dog's position did not permit simultaneous visualization of both lobar fields.
29. We thank A. Purgue, E. Wu, and E. L. Brainerd for critical technical assistance. J. Feller, W. Palmer, R. Bonofacio, and J. Ogelsby performed kinematic analyses. We are grateful to C. R. Taylor and the staff of the Concord Field Station and to A. L. Lage, D. Ashford, L. A. Trudell, T. J. Roberts, C. T. Farley, and R. Kram for assistance with the dog experiments; S. B. Filan and A. J. Werth for laboratory work; L. L. Meszoly for rendering the illustrations; and A. H. Coleman for photography. D. F. Boggs, D. E. Leith, C. R. Taylor, and S. M. Tenney provided useful critiques. This study was supported by NIH grant BRSG S07 RR07092 to the University of Utah and NSF grant DIR-9001699 to Harvard University.

16 April 1993; accepted 18 August 1993

Resistance of Mice Deficient in IL-4 to Retrovirus-Induced Immunodeficiency Syndrome (MAIDS)

Osami Kanagawa,* Barbara A. Vaupel, Shinyo Gayama, Georges Koehler, Manfred Kopf

The murine acquired immunodeficiency syndrome (MAIDS) is induced by a defective murine leukemia virus and has many symptoms similar to those found in patients infected with the human immunodeficiency virus. The presence of both B cells and CD4$^+$ T cells is critical for the development of the disease. Furthermore, a Th2 cytokine response dominates during the progression of the disease. When interleukin-4 (IL-4)–deficient mice that are defective in Th2 cytokine responses were infected, there was no lethality, and the development of the T cell abnormalities associated with MAIDS was delayed. These data suggest that IL-4 or a Th2 response is involved in the development of retrovirus-induced immunodeficiency in mice.

During MAIDS progression, abnormal functioning of CD4$^+$ T cells is observed, including loss of proliferative capacity and IL-2 production in response to mitogens and antigens as well as impaired help for the induction of cytolytic T lymphocyte responses (*1*). At later times after infection, T cells specifically produce IL-4 and IL-10 and low amounts of interferon-γ, which is characteristic of a dominant Th2 response (*2*). This suggests that Th2 cytokines may determine the fatal outcome of the disease.

To investigate the role of IL-4 and Th2 cytokines in MAIDS development, we used IL-4–deficient mice, which carry a targeted disruption of the gene encoding IL-4 as a result of homologous recombination in embryonic stem cells (*3*). The IL-4–deficient (IL-4$^{-/-}$) and control (IL-4$^{+/+}$) mice (F_2 interbreeding from 129/Sv × C57B1/6) were infected with LP-BM5 virus, as a mixture of replication-competent and replication-defective murine leukemia viruses produced by SC-1 cells (*4*). The development of lymphoadenopathy, T cell function, and mortality was monitored. From 6 to 20 weeks after infection, 28 out of 28 IL-4$^{+/+}$ mice progressively developed visible lymph node enlargement at the cervical and axillar regions (Table 1). In contrast, 1 out of 24 and 3 out of 24 IL-4$^{-/-}$ mice developed lymphoadenopathy at 12 and 20 weeks, respectively, after infection. The development of splenomegaly in infected IL-4$^{+/+}$ mice was observed as a 10- to 12-fold increase in the number of spleen cells as compared with that in uninfected controls. In contrast, the number of spleen cells in infected IL-4$^{-/-}$ mice increased less than twofold (Table 2). To further examine T cell function, we stimulated spleen cells with either monoclonal antibody to the T cell receptor (anti-TCR) or phorbol 12-myristate 13-acetate (PMA) plus ionomycin and assessed the cells for IL-2 production. By 8 weeks after infection, spleen cells from IL-4$^{+/+}$ mice were no longer able to produce IL-2 in response to both PMA plus ionomycin and anti-TCR stimulation (Table 2). In contrast, spleen cells of infected IL-4$^{-/-}$ mice remained functionally intact. However, T cells from one IL-4$^{-/-}$ mouse that developed lymphoadenopathy more than 20 weeks after infection also were unable to respond to anti-TCR and anti-CD3 in vitro (*5*). All IL-4$^{+/+}$ mice infected with LP-BM5 virus died within 25 weeks after infection, whereas none of the IL-4$^{-/-}$ mice died during this period of time (Fig. 1). These results demonstrate that IL-4–deficient mice are resistant to the development of MAIDS virus–induced disease.

We next determined the surface phenotype of lymph node T cells in mice infected with LP-BM5 virus. Although the percent-

O. Kanagawa, B. A. Vaupel, S. Gayama, Department of Pathology and Medicine, Washington University School of Medicine, St. Louis, MO 63110.
G. Koehler and M. Kopf, Max Planck Institute for Immunobiology, Stuebeweg 51, D-7800 Freiburg, Germany.
*To whom correspondence should be addressed.

Table 1. Resistance of IL-4–deficient mice to infection with LP-BM5. LP-BM5 virus produced by chronically infected SC-1 cells was inoculated intraperitoneally (0.5 ml) into young (4- to 5-week-old) IL-4$^{-/-}$ and IL-4$^{+/+}$ mice. Mice were monitored daily for the development of lymphoadenopathy at the inguinal, axillar, and cervical lymph nodes.

Mice	Mice with lymphoadenopathy/mice infected			
	6 weeks	8 weeks	12 weeks	20 weeks
		Experiment 1		
IL-4$^{-/-}$	0/12	0/12	0/12	2/12
IL-4$^{+/+}$	7/12	11/12	12/12	3/3*
		Experiment 2		
IL-4$^{-/-}$	0/12	0/12	1/12	1/12
IL-4$^{+/+}$	15/16	16/16	16/16	16/16

*Only three mice survived to this point.